Dating the northwest shelf of Australia since the Pliocene

Groeneveld[1,2*], J., D. De Vleeschouwer[3], J. C. McCaffrey[4], S. J. Gallagher[4]

[1]Alfred Wegener Institute, Helmholtz Center for Polar and Marine Research, Telegrafenberg A45, D-14473 Potsdam, Germany

[2]Department of Geosciences, University of Bremen, Leobener Strasse, D-28359 Bremen, Germany

[3]MARUM-Center for Marine Environmental Sciences, University of Bremen, Klagenfurter Strasse 2-4, D-28359 Bremen, Germany

[4]School of Earth Sciences, The University of Melbourne, Melbourne, Victoria, 3010, Australia

*Corresponding author: jgroeneveld@uni-bremen.de

ORCID:

JG: 0000-0002-8382-8019

DDV: 0000-0002-3323-807X

JCM: 0000-0001-7714-3956

SJG: 0000-0002-5593-2740

Keywords: benthic foraminiferal isotopes, seismic network, downhole wireline logging, NW-Australia, planktonic foraminiferal biostratigraphy

Abstract

Accurate dating of marine sediments is essential to reconstruct past changes in oceanography and climate. Benthic foraminiferal oxygen isotope series from such sediments record long-term changes in global ice volume and deep-water temperature. They are commonly used in the Plio-Pleistocene to correlate deep ocean records and to construct age models. However, continental margin settings often display much higher sedimentation rates due to variations in regional depositional setting and local input of sediment. Here, it is necessary to create a regional multi-site framework to allow precise dating of strata. We create such a high-resolution regional framework to determine the ages of events for the Northwest Shelf (NWS) of Australia, which was cored by International Ocean Discovery Program (IODP) Expedition 356. We employ benthic foraminiferal oxygen and carbon isotopes to construct an astronomically-tuned age model for IODP Site U1463. The age model is applied to the IODP Site U1463 downhole-logging natural gamma radiation (NGR) depth-series, which was then correlated to the NGR of other IODP sites and several industry wells in the area. The IODP Site U1463 age-depth model provides geologic time anchors for numerous sedimentary archives on the NWS. This approach allows assigning ages to regional seismic reflectors and the timing of key climate-related siliciclastic phases in a predominantly carbonate-rich sequence like the

Bare Formation. Finally, this age model is used to chronologically calibrate planktonic foraminiferal biostratigraphic datums showing that the Indonesian Throughflow (ITF) had shoaled enough during the early Pliocene to act as biogeographical barrier between the Pacific and Indian Ocean.

Plain Language Summary

Determining the age of marine sediments is essential to reconstruct past changes in oceanography and climate. The oxygen isotopes of benthic foraminifera record long-term changes in global ice volume and deep-water temperature, and are commonly used to construct age models. However, continental margin settings often display much higher sedimentation rates due to regional input by rivers. Here, it is necessary to create a regional framework to allow precise dating of strata. We created such a framework for the Northwest Shelf (NWS) of Australia, which was cored by International Ocean Discovery Program (IODP) Expedition 356. We used oxygen and carbon isotopes in benthic foraminifera to construct an astronomically-tuned age model for IODP Site U1463. The natural gamma radiation (NGR) variations for IODP Site U1463 were then correlated to those of other IODP sites and industry wells in the area. The IODP Site U1463 age-depth model thus provides a reference for other archives on the NWS allowing to assign ages to regional seismic reflectors and the timing of sediment input via rivers. This age model is also used to determine first and last occurrences of foraminifera showing that the Indonesian Throughflow (ITF) blocked the migration of foraminifera from the Pacific to the Indian Ocean after 5 Ma.

1. Introduction

Accurate dating of marine sediments is essential to reconstruct past changes in oceanography and climate (Lisiecki and Lisiecki, 2002; Huybers and Wunsch, 2004; Bronk Ramsey, 2009). Global stacks, compilations or splices of long-term oxygen isotope records related to ice volume and temperature are commonly applied to correlate deep ocean records, and to construct age models (Zachos et al., 2001; Lisiecki and Raymo, 2005; De Vleeschouwer et al., 2017). However, for regional continental settings with high sedimentation rates such stacks cannot always be used, because they cannot be linked directly to a global stack such that it is therefore necessary to create a regional framework to allow precise correlation.

The NWS of Australia is an ideal place to study the effects of global climate and ocean change. It lies directly downstream of the Indonesian Throughflow (a major branch of the global thermohaline conveyor) and is under the direct influence of the Australian Monsoon (Gallagher et al. al., 2017). The long history of intense hydrocarbon exploration using large seismic and well datasets (Longley et al., 2002) and a recent International Ocean Discovery Program (IODP) Expedition (Gallagher et al., 2017) have revealed the existence of thick (> 2 km) sequences of Cenozoic to Recent upper bathyal to shelfal marine strata (see summaries in Keep et al., 2018; deMenocal and Gallagher 2019). These strata record long and short-term climate/ocean variability (Moss et al., 2004; Gallagher et al., 2009; Christensen et al., 2017; Groeneveld et al., 2017; De Vleeschouwer et al., 2018; 2019; Ishiwa et al., 2019; Auer et al., 2019) and have increased our understanding of reef evolution (Gorter et al., 2002; Power, 2008; Ryan et al., 2009; Rosleff-Soerensen et al., 2012; Gallagher et al., 2014; McCaffrey et

al., 2020) and subtropical to tropical siliciclastic/carbonate platform development (Cathro et al., 2003; Sanchez et al., 2012; Goktas et al., 2016; Gallagher et al., 2018; Tagliaro et al., 2018; Anell and Wallace, 2019). In addition, these strata host substantial mass-transport deposits (with volumes ~17 to >162 km^3) (Hengesh et al., 2013; Scarselli et al., 2013) that were triggered by ongoing neo-tectonism as the Australian plate is colliding with the Asian plate (Keep et al., 2018) or subsidence variability (Gurnis et al., 2020).

Analyses of industry seismic and downhole log datasets/samples have contributed significantly to our knowledge of the Cenozoic evolution of the NWS. However, until IODP Expedition 356 (Gallagher et al., 2017) the only samples of the upper Cenozoic strata of the region were cuttings, sidewall cores (Wallace et al., 2003; Moss et al., 2004; Rosleff-Soerensen et al., 2012; Gallagher et al., 2009), limited engineering cores of the upper 80 m (Collins, 2002: Gallagher et al., 2014) and samples of the modern sedimentary veneer (Jones, 1973; James et al., 2004).

IODP Expedition 356 continuously cored up to 1 km of Miocene to Recent strata in four sites from the Northern Carnarvon and Roebuck basins to document Indonesian Throughflow (ITF) evolution, long-term variations in Australian monsoon precipitation, and the establishment of continental aridity (Gallagher et al., 2017; Fig. 1). A suite of downhole logs was obtained from each site including seismic velocity data. These wireline logs are directly comparable to regional data from industry wells (Gallagher et al., 2014) and can be used to map subsurface reflectors in 2D seismic data (cf. McCaffrey et al., 2020).

In this work, we construct an astronomically-tuned, and therefore independent, age model for IODP Site U1463 based on benthic foraminiferal $\delta^{18}O$ and $\delta^{13}C$ records. We then extrapolate the IODP Site U1463 age model to other IODP Expedition 356 sites, as well as to regional industry wells and to 2D seismic data. This approach ultimately results in a consistent age model for late Neogene strata on the NWS of Australia. The correlation of Neogene stratigraphy among industry wells and IODP Expedition 356 sites is achieved by using natural gamma radiation (NGR) wireline logs. Distinct marker beds and their geological ages are then mapped throughout regional 2D seismic lines along the NWS. This regional and seismically tied Neogene age model can be used to improve age constraints on subsurface reef and carbonate platform development (e.g. McCaffrey et al., 2020), mass transport deposit generation and periodicity, and the evolution of major siliciclastic pulses (e.g. the Bare Formation; Tagliaro et al., 2018) related to regional (and global) climate and oceanic events. Additionally, the independent age model is used to establish a high-resolution planktonic foraminiferal biostratigraphy allowing comparison to published biohorizons from the latest Miocene into the Pleistocene.

2. Material and methods

2.1 Site selection

We selected a series of IODP sites and industry wells to establish a consistent framework for dating the NWS (Fig. 1; Table 1). IODP Site U1463 in the Northern Carnarvon Basin was selected as reference site for the NWS of Australia as this site contains a continuous, high-resolution record of deeper water sediments from the Mio-Pliocene transition into the Pleistocene (Gallagher et al., 2017). A high-resolution benthic stable oxygen and carbon isotope record was established for this

site and astronomical tuning was performed to provide an independent age model for the NWS. The NGR record was then used for correlation to the other IODP sites and the industry wells. Additionally, this age model was used to confirm and/or determine important biostratigraphic datums for planktonic foraminifera for this section of the Indian Ocean.

IODP Site U1462 in the Northern Carnarvon Basin and IODP Site U1464 in the Roebuck Basin are included as part of a parallel section along the NWS (Fig. 1). For all these sites NGR records are available and can therefore be correlated to the reference NGR record of IODP Site U1463 (Gallagher et al., 2017). Additionally, we included a series of industry wells on the NWS to expand the coverage on the NWS (Fig. 1; Table 1). The wells were selected based on their previous use as downcore record/paleoceanographic reconstruction, and for having representative NGR records to allow correlation with the IODP sites (Gallagher et al., 2014).

Table 1) Overview of IODP sites and industry wells used in this study.

Site	IODP Exp. 356	Industry Well	Latitude	Longitude	Present-day water depth (m)
U1462C[1]	x		19°49.28'S	115°42.62'E	87
U1463B[2]	x		18°57.92'S	117°37.43'E	145
U1464C	x		18°03.92'S	118°37.89'E	264
Finucane-1		x	19°17.34'S	116°45.96'E	139
Angel-2		x	19°27.90'S	116°39.48'E	87
Goodwyn-6		x	19°43.32'S	115°51.30'E	124
Goodwyn-2		x	19°39.78'S	115°51.96'E	133

[1]within 150 m of Fisher-1 industry well.

[2]within 150 m of Picard-1 industry well.

2.2 Benthic stable oxygen and carbon isotopes

The shipboard biostratigraphy (Gallagher et al., 2017; Christensen et al., 2017) provided the necessary time markers to inform a sampling strategy that allows for the construction of an astronomically-tuned age model (30-40 cm sampling resolution, corresponding to ~6 kyr temporal resolution) (Fig. 2). Samples were freeze-dried, subsequently washed over a 63 µm mesh sieve and oven-dried. *Uvigerina* spp. was selected for performing stable oxygen and carbon isotopes. Up to 20 specimens were picked from the 250-400 µm size fraction, which was extended to 150-250 µm when not enough specimens were present. Stable isotope analyses were performed on a Finnigan MAT 251 gas isotope ratio mass spectrometer equipped with an automated carbonate preparation device at MARUM, University of Bremen. Isotopic results were calibrated relative to the Vienna Pee Dee belemnite (VPDB) using the NBS19 standard. The standard deviation of the house standard (Solnhofen limestone) was 0.03‰ for $\delta^{13}C$ and 0.04‰ for $\delta^{18}O$ during the measuring period.

2.3 Biostratigraphy

Dried samples were sieved over a 150 µm mesh size before identification of specific marker species. A total of 121 samples of IODP Site U1463 (section 356-U1463-C-20-H4 (188.05 m CCSF) to section 356-U1463-C-56-F3 (401.78 m CCSF)) were investigated for specific species of planktonic foraminifera to determine if their published biostratigraphic first and/or last occurrences agree with published datums for the Atlantic and Pacific (Table 2). Planktonic foraminifera were identified following the taxonomy of Kennett and Srinivasan (1983), Bolli and Saunders (1985), Schiebel et al. (2017), and Microtax (www.mikrotax.org/pforams). Published ages for bio-events are from Gradstein et al. (2012) and Wade et al. (2011). Individual foraminifera were recorded in qualitative terms based on an assessment of all grains from the 150-250 µm, 250-400 µm, and >400 µm size fractions loosely covering a picking tray. The relative abundance of specific foraminiferal species within the assemblage was classified as common, possibly present, or in absolute numbers to determine ratios (e.g. sinistral vs dextral for *Pulleniatina* spp.). Due to the occasional poor preservation of the sample material it was not always possible to determine if a certain species was present in a particular sample (Gallagher et al., 2017). Preservation was classified from (very) poor via medium to (very) good. New ages for the respective biostratigraphic datums are based on the independently, orbitally-tuned benthic isotope age model for IODP Site U1463 (Table 2).

Table 2) Shipboard biostratigraphic age model for IODP Site U1463 in comparison with the updated biostratigraphic datums based on the new astronomically-tuned age-depth model, as well as the geological timescale, ODP Site 763, and Deep Sea Drilling Program (DSDP) sites 214 and 586.

	This study[1]			**Shipboard IODP Exp. 356**		**Geological Timescale**	**DSDP Site 214**	**ODP Site 763**	**DSDP Site 586**
Marker species	**Sample**	**Depth CSF-A (m)**	**Age (Ma)[2]**	**Sample**	**Depth CSF-A (m)**	**Age (Ma)[3]**	**Age (Ma)[4]**	**Age (Ma)[5]**	**Age (Ma)[4]**
Top *G. fistulosus*	356-U1463C-20H-4-125	178.35	1.69	356-U1463C-24H-CC	220.54	1.88		1.73	
Top *G. limbata*	356-U1463D-22H-2-85	191.75	1.84	356-U1463C-24H-CC	220.54	2.39		2.10	
Base *G. inflata*	356-U1463D-22H-6-45	197.35	1.91					2.58	
Top *G.extremus*	356-U1463D-23H-3-45	202.35	1.97	356-U1463C-21H-CC	192.05	1.99		1.87	
Top *G. exilis*	356-U1463C-23H-4-125	206.85	2.04			2.10			
Base *G. truncatulinoides*	356-U1463C-24H-1-125	211.85	2.16	356-U1463C-20H-CC	182.24	1.93		2.10	
Top *G. pseudomiocenica*	356-U1463C-24H-3-5	213.65	2.18			2.30			
Top *G. woodi*	356-U1463C-26H-4-5	234.15	2.51			2.30			
Top *D. altispira*	356-U1463C-27H-4-125	242.85	2.70	356-U1463C-29H-CC	265.63	3.46[6] 3.05[6] 3.11[6]		3.05	
Base *G. tosaensis*	356-U1463B-29H-2-89	258.35	3.06	356-U1463C-26H-CC	238.89	3.35		2.84	
Top *G. margaritae*	356-U1463C-29H-5-42	262.55	3.13	356-U1463C-36F-4	301.75	3.85		3.38	
Top *S. kochi*	356-U1463C-29H-5-42	262.55	3.13[7]	356-U1463C-46F-3	334.71	4.53		3.35	
Base *G. fistulosis*	356-U1463B-29H-5-5	262.05	3.16					3.26	
Top *S. seminulina*	356-U1463C-30H-2-42	267.55	3.34	356-U1463B-36X-CC	308.11	3.58		3.35	
Top *P. primalis*	356-U1463C-30H-3-43	269.05	3.36	356-U1463C-30H-6	273.88	3.66		2.84	
Top *G. plesiotumida*	356-U1463C-30H-3-43	269.05	3.36			3.76	3.75	2.39	3.30

Base *S. dehiscens*	356-U1463B-31F-2-89	273.55	3.45			5.48	4.70	3.58	4.30
Base *G. ruber*	356-U1463C-32F-1-130	281.95	3.57						
Base *P. obliquiloculata*	356-U1463C-32F-3-5	283.75	3.60				4.10	3.33	3.70
Top *G. crassula*	356-U1463C-37F-1-125	302.95	4.03						
X *Pulleniatina* sin to dex	356-U1463C-37F-4-45	306.25	4.08	356-U1463B-36X-CC	308.11	4.08			
Top *G. nepenthes*	356-U1463C-40F-2-85	314.15	4.20			4.36	3.90	3.44	4.30
Base *G. crassula*	356-U1463C-44F-4-5	328.04	4.43						
Base *G. crassaformis*	356-U1463C-48F-1-45	339.25	4.64			4.30	3.85	4.41	3.20

[1]Raw data are available at https://doi.pangaea.de/10.1594/PANGAEA.921913

[2]Age based on the new, orbitally-tuned age model for IODP Site U1463

[3]Age as in Wade et al. (2011) and Gradstein et al. (2012)

[4]Srinivasan and Sinha (1998; DSDP Site 214 and DSDP Site 586)

[5]Sinha and Singh (2008; ODP Site763)

[6]3.46 Ma (Wade et al., 2011 - Pacific); 3.05 Ma (Shackleton et al., 1995 - Pacific); 3.11 Ma (Wade et al., 2011 - Atlantic)

[7]A similar occurrence was found at IODP Site U1482 (Rosenthal et al., 2018)

2.4 Natural Gamma Radiation Downhole Logging

Downhole logging formed an indispensable part of scientific data acquisition during IODP Expedition 356, with downhole logging performed at five out of a total of seven sites (Gallagher et al., 2017). In this paper, we incorporate downhole logging records from IODP sites U1462, U1463 (Northern Carnarvon Basin) and U1464 (Roebuck Basin). The natural gamma radiation (NGR) logs of the latter two sites have been used for paleoclimate studies in Christensen et al. (2017) and Groeneveld et al. (2017) respectively, and a detailed description of the NGR downhole logging methodology during IODP Expedition 356 can be found in these two studies.

We complement the IODP NGR downhole logs with wireline log data from the latest Miocene to Pleistocene sections of four industry wells from the Northern Carnarvon Basin (Fig. 1, 3; Table 1). From east to west, these industry wells are Finucane-1, Angel-2, Goodwyn-6, and Goodwyn-2; their well logs can be sourced from the Geoscience Australia online NOPIMS database (http://www.ga.gov.au/nopims; last access 21 May 2020). We interpreted the approximate stratigraphic position of the latest Miocene in the industry wells by using previously-published biostratigraphic data from cuttings by Gallagher et al. (2009, 2014) and by extrapolating from the detailed IODP age-depth models in the Carnarvon Basin.

We established a detailed correlation between the three IODP and four industry NGR downhole logs by applying a dynamic time warping approach. Dynamic time warping (DTW) is a technique to compare depth- or time-series with each other. The objective of DTW is, given two complementary series, to stretch or compress them locally in order to make one resemble the other as much as

possible. Hence, the warping refers to the optimal deformation of the depth- or time-scale of one of the two input series to match the other. In a geologic context, DTW can be very useful, as the technique can incorporate constraints on stratigraphic ages and realistic sedimentation rates (Kotov and Pälike, 2017; Lisiecki and Lisiecki, 2002; Lisiecki and Herbert, 2007). In this study, we compute dynamic time warps and optimal alignments between NGR-logs by using the open-source R package dtw by Giorgino (2009) on the R platform for statistical computing (R Core Team, 2014). Thereby, we always use the IODP Site U1463 computed gamma ray emission (HCGR) measured in American Petroleum Institute units (gAPI) as the reference. The depth-scales of the two other IODP Sites and four other industry wells are thus warped, so to display an optimal NGR-series fit with IODP Site U1463 (Fig. 3 and Suppl. Fig. 1). During DTW, we use the slope-constrained step patterns from Sakoe and Chiba (1978) to place bounds on the local slope of the warping curve. Therewith, we avoid the situation where local sedimentation rates exhibit unrealistic deviations from the mean sedimentation rate. After DTW, we tested whether the generated mapping function between the depth-series under investigation and IODP Site U1463 fulfills biostratigraphic and lithostratigraphic scrutiny. When this was not the case, we reiterated DTW with adjusted settings, for example by tightening or relaxing sedimentation rate constraints or by adjusting the presumed stratigraphic position of the latest Miocene in the industry wells. In a final step we projected the biostratigraphic datums determined at IODP Site U1463 onto the other sites following the DTW correlations. As these correlations are based on U1463 wireline depth below the seafloor (WMSF) and the biostratigraphic datums are reported in U1463 cored depth (CSF-A), this projection involved a conversion of the U1463 depth scale from cored to wireline depth (WMSF). After this conversion, the U1463 biostratigraphic datums were projected along our DTW correlations determining approximate positions of the respective biostratigraphic datums at each site (Table 3). We emphasize that this projection does not classify as a new age model for the other sites but rather predicts the expected position of different biostratigraphic datums.

The measurement of depth is an essential obstacle in sub-surface marine geology. Next to the two-way travel time in seismic images, this study uses three different depth-scales for isotopic and NGR depth-series.

1. Industry wireline NGR logs are reported along a depth-scale in meters below rotary table (mbrt) from which the well was drilled. This depth scale thus also includes the full depth-range of the water column and the height of the rotary table above mean sea-level. Sources of error in this depth-scale are related to uncompensated heave in case of floating rigs, stretching of the wireline cable and stick and slip of the downhole tool.

2. IODP wireline NGR logs are reported using a Wireline log Matched depth below Sea Floor (WMSF) depth scale. Water depth and rig height are excluded by identifying the sea floor by means of a stepwise increase in the NGR signal at the sea bed. The uncertainty on this determination adds to the above-mentioned sources of error.

3. We report benthic isotope data, measured on IODP core samples, along the Core Composite depth below Sea Floor (CCSF) depth scale. This depth scale considers adjusted depths constructed to resolve gaps in the core recovery and depth inconsistencies. Typically, scientists construct a CCSF scale onboard a research vessel like JOIDES Resolution by shifting cores vertically based on the correlation of high-resolution core logging data from multiple, adjacent holes. In this instance, for IODP Site U1463, we use the shipboard splice, with the slight revision in the Pliocene, as reported in De

Vleeschouwer et al. (2018). At IODP Site U1463, the WMSF depth is consistently shallower than the CCSF scale: The offset between wireline and coring depth varies from 15 to 38 m and may be explained by sediment expansion in the drilling process.

Table 3) Tie-points (WMSF depth scale for IODP sites; bRT depth scale for industry wells) for biostratigraphic datums at IODP Site U1463 to other sites on the NWS.

	IODP Site U1463				IODP Site U1462	Goodwyn-2	Goodwyn-6	Angel-2	Finucane-1	IODP Site U1464
Marker Species	**Sample**	**Depth CSF-A (m)**	**Age (Ma)**	**Depth WMSF (m)**	**Depth WMSF (m)**	**Depth bRT (m)**	**Depth bRT (m)**	**Depth bRT (m)**	**Depth bRT (m)**	**Depth WMSF (m)**
Top *G. fistulosus*	356-U1463C-20H-4-125	178.35	1.69	173.20	457.96	398.94	447.86	345.15	474.18	79.10
Top *G. limbata*	356-U1463D-22H-2-85	191.75	1.84	186.72	474.27	420.76	467.40	367.88	500.47	84.89
Base *G. inflata*	356-U1463D-22H-6-45	197.35	1.91	192.45	484.63	430.71	478.57	379.35	511.94	87.63
Top *G.extremus*	356-U1463D-23H-3-45	202.35	1.97	197.57	495.60	440.95	487.73	389.58	522.17	90.07
Top *G. exilis*	356-U1463C-23H-4-125	206.85	2.04	202.18	505.36	449.25	495.45	398.81	531.39	92.20
Base *G. truncatulinoides*	356-U1463C-24H-1-125	211.85	2.16	207.30	515.42	459.48	503.22	406.75	541.63	94.49
Top *G. pseudomiocenica*	356-U1463C-24H-3-5	213.65	2.18	209.14	520.14	463.16	506.90	410.13	545.30	95.40
Top *G. woodi*	356-U1463C-26H-4-5	234.15	2.51	229.61	565.71	503.95	533.97	434.60	586.24	114.45
Top *D. altispira*	356-U1463C-27H-4-125	242.85	2.70	238.63	592.07	522.00	547.14	451.28	601.67	127.25
Base *G. tosaensis*	356-U1463B-29H-2-89	258.35	3.06	255.21	630.48	555.14	572.97	478.73	632.87	149.20
Top *G. margaritae*	356-U1463C-29H-5-42	262.55	3.13	259.55	641.15	563.84	580.60	484.59	641.56	153.92
Top *S. kochi*	356-U1463C-29H-5-42	262.55	3.13[7]	259.55	641.15	563.84	580.60	484.59	641.56	153.92
Base *G. fistulosis*	356-U1463B-29H-5-5	262.05	3.16	259.04	639.01	562.80	579.93	483.65	640.53	153.47
Top *S. seminulina*	356-U1463C-30H-2-42	267.55	3.34	264.58	652.58	573.89	587.51	491.35	651.00	158.50
Top *P. primalis*	356-U1463C-30H-3-43	269.05	3.36	266.02	657.45	576.77	590.03	492.14	653.27	159.11
Top *G. plesiotumida*	356-U1463C-30H-3-43	269.05	3.36	266.02	657.45	576.77	590.03	492.14	653.27	159.11
Base *S. dehiscens*	356-U1463B-31F-2-89	273.55	3.45	270.33	669.80	584.87	594.20	498.03	661.90	163.53

Base *G. ruber*	356-U1463C-32F-1-130	281.95	3.57	278.39	681.53	596.18	598.22	502.82	673.75	167.79
Base *P. obliquiloculata*	356-U1463C-32F-3-5	283.75	3.60	280.11	682.60	598.75	599.08	503.68	676.66	168.55
Top *G. crassula*	356-U1463C-37F-1-125	302.95	4.03	298.44	701.95	621.19	613.45	512.99	691.68	177.55
X *Pulleniatina* sin to dex	356-U1463C-37F-4-45	306.25	4.08	301.57	703.33	627.46	618.32	515.17	694.37	180.75
Top *G. nepenthes*	356-U1463C-40F-2-85	314.15	4.20	309.74	709.12	640.95	632.27	519.64	701.96	187.30
Base *G. crassula*	356-U1463C-44F-4-5	328.04	4.43	324.45	716.89	649.07	640.00	527.07	712.24	195.68
Base *G. crassaformis*	356-U1463C-48F-1-45	339.25	4.64	335.80	725.27	663.15	651.42	532.75	722.44	202.08

2.5 Seismic correlation and age determination

Extensive publicly released petroleum exploration multichannel seismic surveys are available for the NWS for our 2D seismic analyses (Longley et al., 2002), which have been provided by Geoscience Australia (http://dbforms.ga.gov.au/www/npm.well.search; latest access 7 June 2020). These industry seismic data have been extensively used in previous studies to document the Paleogene to Neogene evolution of the carbonates and siliciclastics along this margin (e.g. Rosleff-Soerensen et al., 2012; Belde et al., 2017; McCaffrey et al., 2020). Key seismic reflectors in these datasets were previously assigned ages based on either biostratigraphy (Gallagher et al., 2014; Belde et al., 2017; McCaffrey et al., 2020) or Sr-isotope ages (Rosleff-Soerensen et al., 2012). In this study we use the ages determined by the benthic foraminiferal isotope, orbitally-tuned age model.

We constructed two composite seismic profiles; one parallel along the NWS connecting the different IODP sites and industry wells, and one perpendicular to IODP Site U1463 to show the 3D-presence of the main features on the NWS (Fig. 4, 5). The WMSF depth scale was converted to a two-way travel time (TWT) scale using downhole velocity (check-shot) data to allow the ages to be plotted on seismic profiles. In the absence of check-shot velocity data, correlation to the TWT scale is calculated by cumulatively adding sonic travel times between each downhole P-wave velocity measurement. Industry well depths were correlated to the TWT scale using the calibrated check-shot data and Vertical Seismic Profiles (VSP) from Industry well completion reports. Seismic correlation and identification of characteristic features were performed using the IHS Markit Kingdom software using standard criteria for identification (Mitchum Jr. et al., 1977). The characteristic horizons H5 (Tortonian), H6 (Base Pliocene), and H7 (Base Pleistocene) were used as baseline to correlate the different seismic profiles (Belde et al., 2017; McCaffrey et al., 2020).

3. Results and Discussion

3.1 Orbitally-tuned age model based on benthic stable isotopes

The initial age model for IODP Site U1463 was based on shipboard data, specifically the biostratigraphy using nannofossils and planktonic foraminifera (Gallagher et al., 2017; Christensen et al., 2017). This showed that a complete latest Miocene to Pleistocene sediment sequence is present at IODP Site U1463. Stable oxygen and carbon isotopes using the planktonic foraminifer *Trilobatus sacculifer* showed that the $\delta^{13}C$ record exhibited the 405 kyr eccentricity cyclicity that could be correlated to the astronomical solution (Laskar et al., 2004; De Vleeschouwer et al., 2018). The completeness of the IODP Site U1463 sediment archive and its clear link to global insolation patterns means it can be used as the reference age model for the NWS of Australia.

Benthic stable oxygen isotope data are commonly used to construct Plio-Pleistocene age models as they contain the global signature of climatic and oceanographic change through time (Lisiecki and Raymo, 2005). The main premise of these type of data is that the benthic foraminifera live at water depths where local changes in water mass characteristics are only minor, and thus the global signal is the main control on this proxy. Paleo-water depths for IODP Site U1463 during the Pliocene and early Pleistocene, however, were never deeper than ~600 m, which means that bottom waters may have experienced significant changes in temperature and salinity affecting the $\delta^{18}O$-signature of benthic foraminifera (Gallagher et al., 2017; Gurnis et al., 2020). Additionally, ice volume changes during the early Pliocene, and thus variations in benthic $\delta^{18}O$, were not very pronounced (Lisiecki and Raymo, 2005). Instead of $\delta^{18}O$-based correlation, we use the strong imprint of 405-kyr eccentricity in the *Uvigerina* spp. $\delta^{13}C$ record at IODP Site U1463. Taking into account bio- and magnetostratigraphic constraints, these 405-kyr eccentricity cycles correspond to the 5th - 12th eccentricity cycle counting back from the present (Fig. 2; Laskar et al., 2004). Only in a second step, we correlate the benthic $\delta^{18}O$ record at IODP Site U1463 to the LR04 benthic isotope stack (Fig. 2; Lisiecki and Raymo, 2005). In the younger part of the age model, i.e. after the onset of Northern Hemisphere Glaciation (<2.7 Ma), we additionally used the strong expression of glacial-interglacial oscillations in the TEX86 sea water temperature record of IODP Site U1463 to fine-tune the age model (Smith et al., subm.). The 29 tie-points between depth and time define the age-depth model of IODP Site U1463 and imply sedimentation rates between 4 and 8 cm/kyr throughout the studied interval (Table 4) with rapidly increasing sedimentation rates in the youngest part of the record. The age model in this study is similar yet temporally more comprehensive than previous IODP Site U1463 age models presented in De Vleeschouwer et al. (2018) and Auer et al. (2019).

Table 4) Tie-points of reconstructed age vs sediment depth based on benthic stable oxygen and carbon isotopes of IODP Site U1463.

Depth (m CCSF-a)	Age (ka)		Depth (m CCSF-a)	Age (ka)
162.23	1509.36		318.10	3763.68
174.20	1586.37		325.85	3966.33
185.84	1666.14		330.44	4040.77
200.76	1794.32		338.27	4157.76
222.61	2071.61		342.53	4228.86
228.43	2162.55		354.41	4373.94
237.34	2283.15		373.54	4691.36
244.87	2376.48		386.12	4893.50
256.04	2553.57		392.12	4975.31
270.79	2811.28		401.20	5151.50
284.14	3163.08		412.03	5362.40

291.51	3320.15		415.49	5437.80
301.23	3466.79		419.54	5529.83
310.86	3631.48		422.07	5590.28
315.97	3705.36			

302

303 3.2 Planktonic foraminiferal biostratigraphy

304 Biostratigraphy using planktonic foraminifera is important not only for paleoceanographic
305 reconstructions but also commonly used in the industry for age dating of petroliferous strata. The
306 first appearance and extinction events of different species, known as biohorizons, can be linked to
307 paleomagnetic timescales and orbitally-tuned using benthic foraminiferal $\delta^{18}O$ records to create
308 highly precise age models (Wade et al., 2011; Gradstein et al., 2012). The initial age models for IODP
309 Site U1463 and the nearby IODP sites were only based on the biostratigraphy, as the nature of the
310 carbonate-rich sediments present prevented reliable paleomagnetic analyses (Gallagher et al., 2017).
311 However, not all of these biohorizons are globally synchronous. Isolated basins like the
312 Mediterranean, tectonic obstructions like the closing of oceanic gateways, or climate-induced
313 barriers often show diachroneity of biozonal datums compared to apparently global events. One of
314 the better known and more-recent of these regional bio-events is the disappearance of
315 *Globigerinoides ruber* (pink) in the Indo-Pacific realm 120 kyr ago (Thompson et al., 1979), whereas
316 this taxon still lives today in the Atlantic.

317 Pliocene planktonic foraminiferal biohorizons are mainly calibrated using Pacific or Atlantic studies
318 (Wade et al., 2011; Gradstein et al, 2012 and references therein) and often with differences of up to
319 several 100 kyr (Table 2; Gradstein et al., 2012). These variations hamper the reconstruction of high-
320 resolution paleoceanographic records for the Indian Ocean as it is still unclear which of these
321 biohorizons are applicable to the Indian Ocean. In addition, existing older biostratigraphic studies
322 (e.g. Zachariasse, 1992; Srinivasan and Chaturvedi, 1992; Srinivasan and Sinha, 1998) are often based
323 on out-of-date age models.

324 We document 24 early Pliocene to the early Pleistocene biostratigraphic datums at IODP Site U1463
325 that were determined with an average time resolution of ~28 kyr per sample. The biostratigraphy at
326 IODP Site U1463 can be closely tied to Ocean Drilling Program (ODP) Site 763 further offshore
327 western Australia (Fig. 1; Sinha and Singh, 2008). With a few exceptions, the bio-events are very
328 similar at both locations (Table 2). For example, the final occurrence of *Globigerina nepenthes* (4.20
329 Ma) is ~760 kyr earlier than at ODP Site 763, yet close to the commonly published age (4.36 Ma;
330 Gradstein et al., 2012). As *G. nepenthes* is quite rare at IODP Site U1463, its earlier disappearance
331 may be due to specific local oceanographic conditions. Similarly, *Globorotalia inflata* appears 670 kyr
332 later than at Site 763. This species is often present in upwelling conditions and related to cooler
333 water masses. Accordingly, as *G. inflata* appeared much earlier at ODP Site 763, it implies that this
334 site was affected earlier by the West Australian Current than the more proximal IODP Site U1463, as
335 was suggested by previous reconstructions (Karas et al., 2011; De Vleeschouwer et al., 2018; Auer et
336 al., 2019). Our Indian Ocean biozonal datums at IODP Site U1463 also differ from previous
337 foraminiferal bio-horizons (Table 2; Gradstein et al., 2012; Wade et al., 2011). Similar datum
338 variations are also present at ODP Site 763 and IODP Site U1482 on the Scott Plateau further to the
339 northeast (Rosenthal et al., 2018) suggesting that regional conditions resulted in the temporal
340 variation of particular species. The largest difference is the distribution of *Sphaeroidinella dehiscens*,
341 which has a first occurrence at 5.48 Ma, yet only appears off northwestern Australia at 3.45 Ma

(IODP Site U1463) and 3.58 Ma (ODP Site 763) close to the disappearance of *Sphaeroidinellopsis seminulina* (3.34 Ma). Another important bio-event is the last occurrence of *Dentoglobigerina altispira* at 2.70 Ma. This species is often commonly present throughout the Miocene and Pliocene and its final occurrence is often assigned to be 3.47 Ma (Wade et al., 2011; Gradstein et al., 2012). However, in several locations in the Pacific and Atlantic it was found to have persisted until 3.11-3.13 Ma (Shackleton et al., 1995; Chaisson and Pearson, 1997; Lourens et al., 2004), but rarely in younger strata (Boltovskoy, 1974; Jenkins and Srinivasan, 1986; Shackleton et al., 1995; Norris et al., 1998).

Changes in the coiling direction of certain planktonic species such as the genus *Pulleniatina* spp. may be used as biostratigraphic markers (Saito et al., 1976). The most commonly used datum is the L9-event (100%-sinistral to 100%-dextral) occurring at 4.08 Ma (Saito, 1976; Wade et al., 2011; Gallagher et al., 2017). At Site U1463, the first dextral specimens appear at 4.20 Ma and the last sinistral specimens were present at 3.95 Ma, i.e. a total time span of ~250 kyr for the full change in coiling direction (Table 2) (see raw data in Pangaea). After this change *Pulleniatina* disappears from the Atlantic until 2.26 Ma, yet predominantly dextral forms are still present in the Indian Ocean. At IODP Site U1463 sinistral specimens become common and occasionally dominant again after 2.49 Ma and after 1.76 constitute 100% of the specimens equivalent to Saito's events L4-L8.

The ITF is a major influence on the biostratigraphy in the Indian Ocean as it supplies warm waters from the equatorial Pacific. As the ITF is a relatively shallow current system, sub-surface foraminiferal species are living in water masses, which may originate from the sub-Antarctic or even Atlantic rather than from the Pacific. Srinivasan and Sinha (2000) showed that *Pulleniatina spectabilis*, a commonly occurring Pliocene thermocline species in the equatorial Pacific, never migrated into the Indian Ocean during the Pliocene suggesting that the ITF was already restricted to such an extent that only shallower waters may have passed through it. Indeed, *P. spectabilis* is also not present at IODP Site U1463. However, there is no consistent pattern in offsets between biodatums for other deeper-dwelling species, especially *Globorotalia* spp. at IODP Site U1463 with those in the Atlantic or the Pacific. Some taxa have ages very similar to Atlantic datums, e.g. *Globorotalia exilis*, while others are more similar to Pacific age datums, e.g. *Globorotalia pseudomiocenica*, or somewhere in-between, e.g. *Globorotalia limbata* (Table 2). Although a major switch in the restriction of the ITF occurred 3.5-3.0 Ma when the source waters for the ITF changed from the south Pacific to the north Pacific due to the northward movement of the Australian plate (Cane and Molnar, 2001; Karas et al., 2009), *P. spectabilis* occurred ~5.20-4.20 Ma (Berggren et al., 1985). The lack of a consistent pattern in the biohorizons of deeper-dwelling species during the Pliocene implies that a biogeographical barrier existed prior to the early Pliocene.

One particular biohorizon that may have been established via a different pathway from the Pacific than the ITF is the first occurrence of *Globorotalia truncatulinoides.* This datum is generally placed at 1.93 Ma, however in the southwest Pacific this species had already appeared at ~2.8 Ma (Dowsett, 1989; Lazarus et al., 1995; Spencer-Cervato and Thierstein, 1997). At IODP Site U1463 it appears at 2.16 Ma; this may be due to its migration from the southwest Pacific via the Tasman Leakage (Speich et al., 2002; van Sebille et al., 2012).

3.3 Correlation of NGR between IODP sites and industry wells

Time warping the NGR records of the other Exp. 356 IODP sites and industry wells demonstrates that these sequences have similar downhole gamma ray signatures, compared to IODP Site U1463 (Fig. 3; Christensen et al., 2017). Around the Miocene-Pliocene transition (~5.5 Ma) an increase in NGR was interpreted by these authors to be related to the onset of a wetter climate in northwestern Australia resulting in an increase in river-brought sediments to the NWS due to increasing precipitation. Although a similar increase is seen at most sites investigated, a recent study suggests that this steep increase may not be solely climate related, but rather a tectonic deepening event that did not occur simultaneously in different basins, although this nevertheless created the accommodation space needed to deposit climate-related cyclic sedimentation (Karatsolis et al., 2020). At IODP Site U1464 located in the Roebuck Basin the onset occurs rather abruptly at ~6.0 Ma, while at Site U1463 in the Northern Carnarvon Basin the onset is somewhat later around 5.7 Ma. In addition, all major patterns may be correlated in these different NGR records suggesting a common history and age model. The uppermost part of the NGR records, i.e. above ~80 m, does not show much structure as this part in the NGR signal of the drilling holes is usually impeded by hole casing (Fig. 3).

3.4 Seismic stratigraphic analyses

A series of 2D multichannel seismic profiles were combined to produce a regional composite profile across the NWS connecting several IODP 356 sites (Site U1462 to Site U1464) and industry wells over a distance of ~400 km (Fig. 4). Tracing of seismic reflectors across large distances such as these often encounters many challenges (e.g. condensed surfaces or erosional truncations) when attempted in isolation. However, integration of seismic data with correlated NGR and biostratigraphical data provides regularly distributed control points that allow for accurate tracing of these horizons, even across uncertain sections. This integration between the NGR, biostratigraphy and seismic data provided improved interpretations of previously published seismic horizons (H6 and H7; Belde et al., 2017; McCaffrey et al., 2020) across the shelf, between IODP 356 sites U1462 and U1464.

The transition from the Miocene into the Pliocene is represented across the majority of the shelf between IODP sites U1462 and U1464 by the distinct shift in reflector geometry. This transition, from sets of strong reflectors surrounded by discontinuous zones of disrupted reflectors below the H6 horizon (~6 Ma; Fig. 4), to low amplitude parallel reflectors above, is observed in the well data as a shift in lithology from shallow water carbonate/reefal dominated, to deeper water fine grained sediments. Towards the southern end of the section, the seismic architecture becomes increasingly complex as these sediments are interfingered with the mixed siliciclastic and carbonate Bare Formation (Fig. 4). Between IODP Site U1462 and Angel-2 the Plio-Pleistocene sediments are observed to be underlain by the Bare Formation, placing the top of the Bare Formation at 5.59 Ma at IODP Site U1462. Further north however, between Angel-2 and Finucane-1, a thick siliciclastic package ending at ~2.38 Ma is observed to interfinger with the surrounding Plio-Pleistocene sediments, showing that this formation is non-synchronously deposited along the NWS (Fig. 4). Tagliaro et al. (2018) even identified Bare-like sediments within the overlying carbonates at the nearby industry well Bounty-1 with an age of 1.63 Ma, although the sand layers were minor in comparison with the limestone surrounding them. Further towards the northeast the Cenozoic sediment sequence of predominantly carbonates continues further back in time until the early Cenozoic, although IODP sites U1463 and U1464 only drilled to the early Miocene (Groeneveld et al.,

2017; Gallagher et al., 2017). The depositional setting during the Miocene is generally very shallow with likely subaerial exposure during certain times such that hiatuses may be present.

Additionally, a perpendicular profile crossing the Northern Carnarvon Basin at the location of IODP Site U1463 was constructed showing the general downslope geometry of the shelf (Fig. 5). This profile also shows reef developments during the Miocene, and the presence of a newly identified mass transport deposit on top of the regular sedimentary sequence, called the Picard-slide (Gallagher et al., 2017; Fig. 5).

3.5 Implications for dating the history of the NWS

The creation of a consistent age model for the late Neogene strata on the NWS and its relationship to other subsurface downhole and seismic datasets has allowed us to produce a consistent framework to investigate the evolution of various laterally discontinuous carbonate (tropical reefs) and siliciclastic (the Bare Formation) units that are widespread in this region. After large areas of the NWS were sub-aerially exposed during the late Miocene (Groeneveld et al., 2017; Tagliaro et al., 2018; Petrick et al., 2019), tectonic subsidence during the latest Miocene created sufficient accommodation space to deposit a thick sequence of sediments during the Pliocene and early Pleistocene (Gallagher et al., 2017; Gurnis et al., 2020). This tectonic subsidence is also thought to play a role in the transition of the NWS reef system from primarily barrier reef morphologies in the middle Miocene to pinnacle and atoll formations in the Pliocene (McCaffrey et al., 2020). Our new age framework suggests that deposition of the siliciclastic Bare Formation occurred during the late Miocene and early Pliocene. This unit developed as a fluvial to fluvio-deltaic deposit on a mainly carbonate-dominated shelf (Cathro et al., 2003; Wallace et al., 2003; Sanchez et al., 2012; Tagliaro et al., 2018). Siliciclastic input was especially intense from the Pliocene onwards when climate became wetter (Christensen et al., 2017). The Bare Formation is a laterally discontinuous progradational sand-dominated unit that reached IODP Site U1462 by the earliest Pliocene (Tagliaro et al., 2018). Deposition of the Bare Formation expanded and prograded with the onset of wet climate in northwestern Australia near the base of the Pliocene (5.3 Ma), and deposition continued until climate switched again to dry conditions by the early Pleistocene (2.39-1.93 Ma) (Christensen et al., 2017; Tagliaro et al., 2018). Our new age framework narrowly constrains the age of the termination of this siliciclastic pulse to 2.38 Ma (222 m WMSF in U1463) near Angel-2 (Fig. 3), with remnant siliciclastic deposition continuing until as young as 1.63 Ma at the nearby industry well Bounty-1 (Tagliaro et al., 2018; Fig. 4).

The independent benthic foraminiferal age model for dating the NWS also results in further constraining the ages of seismic reflectors used for regional seismic correlation, e.g. the H6 at ~6 Ma (408 m WMSF in U1463) and H7 at 1.89 Ma (191 m WMSF in U1463) (Belde et al., 2017; McCaffrey et al., 2020; Rosleff-Soerensen et al., 2012).

Our age constrained seismic stratigraphic framework may be applied to most of continental shelf and slope regions of the NWS over an area of ~150,000 km^2. Paleoceanographic drilling has been performed for example on the Wombat Plateau located north of the NWS providing reconstructions going back to the early Cenozoic, but also including detailed studies on the Pliocene and Pleistocene (Exon et al., 1992; Holbourn et al., 2004; Karas et al., 2011). More recently IODP Expedition 363 drilled Sites U1482 and U1483 off the northwestern slope of the NWS in the direct outflow of the

Indonesian Gateway (Rosenthal et al., 2018). However, linking these dated reflectors to deep ocean archive is not straightforward as deep ocean to continental margin linking seismic data are rare. Nevertheless, the NGR and benthic isotope records of the NWS can be correlated allowing a direct link between pelagic paleoceanographic reconstructions and the terrestrial input from Australia to the more proximal locations.

4. Conclusions

On regional scales it is necessary to create a regional framework to allow precise dating of sediments. In this study we have created a high-resolution regional framework to precisely determine the ages of sediments and events on the northwest shelf (NWS) of Australia. This area is ideally located to record changes in the outflow of the Indonesian Throughflow (ITF) as well as to monitor how monsoonal precipitation and aridity change over Australia.

We reconstructed an independent, astronomically-tuned age model based on benthic foraminiferal oxygen and carbon isotopes for International Ocean Discovery Program (IODP) Site U1463. The NGR record for IODP Site U1463 was then correlated to the NGR records of several other IODP sites and industry wells on the NWS. Additionally, these sites were linked to each other using a composite seismic profile along the NWS connecting the main reflectors in the region.

This independently-dated and consistent age framework for the NWS allowed to update existing biostratigraphic datums on planktonic foraminifera, and to fine-tune the ages of the main seismic reflectors and major sedimentary events, e.g. top of the Bare Formation at 2.38 Ma, on the NWS. Biostratigraphic datums of deeper-dwelling planktonic foraminifera show that the ITF had shoaled enough by the beginning of the Pliocene to act as biogeographical barrier. Comparison with regional (ODP Site 763A and IODP Site U1482) and global biostratigraphic events suggests that this area may have provided specific conditions such that some species, i.e. *D. altispira*, *Sphaeroidinellopsis kochi*, and *Globorotalia margaritae*, survived several 100 kyr longer than generally accepted.

We showed how the combination between an independent orbitally-tuned benthic isotope record, downhole records of physical properties and an extensive seismic network, a framework can be created that provides a consistent age model for a specific region. This allows future work in the area, and possibly nearby areas, to be directly linked to this common age framework greatly improving temporal precision.

Acknowledgments

We thank Henning Kuhnert for laboratory assistance. This project was supported by the German Academic Exchange Service (DAAD Project “DANA” ID 57388289 to JG, DDV, JM, and SJG), the German Research Foundation (DFG Project “IDEAL” GR 3528/5-1 to JG). Additional funding to SJG was provided by the Australian IODP office and the ARC Basins Genesis Hub (IH130200012). An Australian Government Research Training Program Scholarship is supporting J. McCaffrey. We would like to thank the IHS Markit for their donation of the Kingdom seismic interpretation software. This research used samples and data provided by the IODP. We thank the JRSO (JOIDES Resolution

Science Operator) staff and the Siem Offshore crew for their invaluable assistance and skill during Expedition 356. Data are stored in the Pangaea database (https://doi.pangaea.de/10.1594/PANGAEA.921913).

References

Anell, I., & Wallace, M.W. (2019). A fine balance: Accommodation dominated control of contemporaneous cool-carbonate shelf-edge clinoforms and tropical reef-margin trajectories, North Carnarvon Basin, NW Australia. *Sedimentology, 67,* 96-117. https://doi.org/10.1111/sed.12628

Auer, G., De Vleeschouwer, D., Smith, R., Bogus, K.A., Groeneveld, J., Grunert, P., Castañeda, I., Patrick, B., Christensen, B.A., Fulthorpe, C.S., Gallagher, S.J., & Henderiks, J. (2019). Timing and pacing of Indonesian Throughflow restriction to Late Pliocene climate shifts. *Paleoceanography and Paleoclimatology*, *34*, 635-657. 10.1029/2018PA003512

Belde, J., Back, S., Bourget, J., & Reuning, L. (2017). Oligocene and Miocene carbonate platform development in the browse basin, Australian Northwest shelf. *Journal of Sedimentary Research, 87*, 795‐816. doi:10.2110/jsr.2017.44

Berggren, W. A., Kent, D. V., & van Couvering, J. A. (1985). Neogene geochronology and Chronostratigraphy. In: Snelling, N. J., ed. The chronology of the geological record: *Geological Society of London Memoir, 10*, 211–250.

Bolli, H.M., & Saunders, J.B. (1985). Oligocene to Holocene low latitude planktonic foraminifera. In Bolli, H.M., Saunders, J.B., and Perch-Nielsen, K. (Eds.), *Plankton Stratigraphy (Vol. 1): Planktic Foraminifera, Calcareous Nannofossils and Calpionellids*. Cambridge (Cambridge Univ. Press), 155–262.

Boltovskoy, E. (1974). Neogene planktonic foraminifera of the Indian Ocean (DSDP Leg 26). In: Davies, T.A., and Luyendyk, B.P. (eds). *Initial Reports of the Deep Sea Drilling Project,* 26. US Government Printing Office, Washington D.C. 675-741.

Bronk Ramsey, Ch. (2009). Dealing with outliers and offsets in radiocarbon dating. *Radiocarbon, 51-3*, 1023-1045.

Cane, M., & Molnar, P. (2001), Closing of the Indonesian seaway as a precursor to east African aridification around 3‐4 million years ago. *Nature, 411*, 157‐162. doi:10.1038/35075500

Chaisson, W.P., & Pearson, P.N. (1997). Planktonic foraminifer biostratigraphy at Site 925: middle Miocene to Pleistocene. In: Shackleton, N.J., Curry, W.B., Richter, C., and Bralower, T.J. (eds). *Proceedings of the Ocean Drilling Program. Scientific Results, 154*. College Station (ODP), TX. 3-31.

Cathro, D.L., Austin, J.A.J.R., & Moss, G.D. (2003). Progradation along a deeply submerged Oligocene-Miocene heterozoan carbonate shelf: How sensitive are clinoforms to sea level variations? *American Association Petrology and Geology Bulletin, 87*, 1547–1574.

Christensen, B.A., Renema, W., Henderiks, J., De Vleeschouwer, D., Groeneveld, J., Castañeda, I.S., Reuning, L., Bogus, K., Auer, G., Ishiwa, T., McHugh, C.M., Gallagher, S.J., Fulthorpe, C.S., & Expedition 356 Scientists (2017). Indonesian Throughflow drove Australian climate from humid

549 Pliocene to arid Pleistocene. *Geophysical Research Letters, 44*, 6914–6925.
550 https://doi.org/10.1002/2017GL072977

551 Collins, L.B. (2002). Tertiary foundations and Quaternary evolution of coral reef systems of Australia's
552 North West Shelf, in: Keep, M., Moss, S.J. (Eds.), *The Sedimentary Basins of Western Australia 3:*
553 *Proceedings of Petroleum Exploration Society of Australia Symposium*. Petroleum Exploration
554 Society of Australia, Perth, Western Australia, 129–152.

555 De Vleeschouwer, D., Vahlenkamp, M., Crucifix, M., & Pälike, H. (2017). Alternating Southern and
556 Northern Hemisphere climate response to astronomical forcing during the past 35 m.y. *Geology*.
557 doi:10.1130/G386663.1

558 De Vleeschouwer, D., Auer, G., Smith, R., Bogus, K.A., Christensen, B.A., Groeneveld, J., Patrick, B.,
559 Henderiks, J., Castañeda, I., O'Brien, E., Ellinghausen, M., Renema, W., Reuning, L., Ishiwa,
560 McHugh, C.M., Gallagher, S.J. & Pälike, H. (2018). The amplifying effect of Indonesian
561 Throughflow heat transfer on Late Pliocene southern Hemisphere climate cooling. *Earth and*
562 *Planetary Science Letters*, *500*, 15-27. doi. 10.1016/j.epsl.2018.07.0350012-821X

563 Dowsett, H.J. (1989). Application of the graphic correlation method to Pliocene marine sequences.
564 *Marine Micropaleontology, 14*, 3-32.

565 Exon, N.F., Borella, P.E., & Ito, M. (1992). Sedimentology of marine Cretaceous sequences in the
566 central Exmouth Plateau (northwest Australia). In: von Rad, U., Haq, B.U., et al. (eds).
567 *Proceedings of the Ocean Drilling Program. Scientific Results, 122*, 233-257.

568 Gallagher, S.J., Wallace, M.W., Li, C.L., Kinna, B., Bye, J.T., Akimoto, K., & Torii, M. (2009). Neogene
569 history of the West Pacific warm pool, Kuroshio and Leeuwin currents. *Paleoceanography, 24*,
570 PA1206. doi:10.1029/2008PA001660

571 Gallagher, S.J., Wallace, M.W., Hoiles, P.W., & Southwood, J.M. (2014). Seismic and stratigraphic
572 evidence for reef expansion and onset of aridity on the Northwest Shelf of Australia during the
573 Pleistocene. *Marine and Petroleum Geology, 57*, 470–481.

574 Gallagher, S.J., Fulthorpe, C.L., Bogus, K.A., Auer, G., Baranwal, S., Castañeda, I.S., B.A.Christensen,
575 Vleeschouwer, D.D., Franco, D.R., Groeneveld, J., M. Gurnis, C.Haller, He, Y., Henderiks, J.,
576 Himmler, T., Ishiwa, T., Iwatani, H., Jatiningrum, R.S., Kominz, M.A., Korpanty, C.A., Lee, E.Y.,
577 Levin, E., Mamo, B.L., H.V. McGregor, C.M.McHugh, Petrick, B.F., Potts, D.C., Rastegar, A., Lari,
578 W., Renema, Reuning, L., Takayanagi, H., & Zhang, W. (2017). *Proceedings of the International*
579 *Ocean Discovery Program, 356*, 1-43. dx.doi.org/10.14379/iodp.proc.356.101.2017

580 Gallagher, S.J., Reuning, L., Himmler, T., Henderiks, J., De Vleeschouwer, D., Groeneveld, J., Rastigar,
581 A., Fulthorpe, C.S., Bogus, K. & Expedition 356 Shipboard Scientists (2018). The enigma of rare
582 Quaternary oolites in the Indian and Pacific Oceans: a result of global oceanographic
583 physicochemical conditions or a sampling bias. *Quaternary Science Reviews*, *200*, 114-122. doi.
584 10.1016/j.quascirev.2018.09.028

585 Gallagher, S.J. & deMenocal, P.B. (2019). Finding dry spells in Ocean Sediments. *Oceanography, 32*
586 (1), 38-41. https://doi.org/10.5670/oceanog.2019.120

Giorgino, T. (2009). Computing and visualizing dynamic time warping alignments in R: the dtw package. *Journal of Statistical Software*, *31*(7), 1-24.

Goktas, P., Austin, J.A., Fulthorpe, C.S., & Gallagher, S.J. (2016). Morphologies and depositional/ erosional controls on evolution of Pliocene-Pleistocene carbonate platforms: Northern Carnarvon Basin, Northwest Shelf of Australia. *Continental Shelf Research, 124*, 63–82. https://doi.org/10.1016/j.csr.2016.05.009

Gorter, J.D., Rexilius, J.P., Powell, S.L., & Bayford, S.W. (2002). Late early to mid-Miocene patch reefs, Ashmore Platform, Timor sea; evidence from 2D and 3D seismic surveys and petroleum exploration wells, in: Keep, M., Moss, S.J. (Eds.), *The Sedimentary Basins of Western Australia 3: Proceedings of Petroleum Exploration Society of Australia Symposium*. Petroleum Exploration Society of Australia, Perth, Western Australia, 355–376.

Gradstein, F.M., Ogg, J.G., Schmitz, M., & Ogg, G. (2012). *The geologic time scale 2012*, Vol. 1. Elsevier, 435p.

Groeneveld, J., Henderiks, J., Renema, W., McHugh, C.M., De Vleeschouwer, D., Christensen, B.A., Fulthorpe, C.S., Reuning, L., Gallagher, S.J., Bogus, K., Auer, G., Ishiwa, T., & Expedition 356 Scientists, 2017. Australian shelf sediments reveal shifts in Miocene Southern Hemisphere westerlies. *Science Advances*, 3, e1602567.

Gurnis, M., Kominz, M., & Gallagher, S.J. (2020). Reversible subsidence on the North West Shelf of Australia. *Earth and Planetary Science Letters, 534*, 116070.

Holbourn, A., Kuhnt, W., Simo, J.A., & Li, Q. (2004). Middle Miocene isotope stratigraphy and paleoceanographic evolution of the northwest and southwest Australian margins (Wombat Plateau and Great Australian Bight). *Palaeogeography, Palaeoclimatology, Palaeoecology, 208*, 1-22.

Hengesh, J.V., Dirstein, J.K., & Stanley, A.J. (2013). Landslide geomorphology along the Exmouth Plateau continental margim, North West Shelf, Australia. *Australian Geomechanics Journal*, Special Offshore Edition, 71-92.

Huybers, P., & Wunsch, C. (2004). A depth-derived Pleistocene age model: Uncertainty estimates, sedimentation variability, and nonlinear climate change. *Paleoceanography, 19*, PA1028. doi:10.1028/2002PA000857

Ishiwa, T., Yokoyama, Y., Reuning, L., McHugh, C.M., De Vleeschouwer, D., & Gallagher, S.J. (2019). Australian summer monsoon variability in the past 14,000 years revealed by IODP Expedition 356 sediments. *Progress in Earth and Planetary Science, 6,* 1-17. doi.org/10.1186/s40645-019-0262-5

James, N.P., Bone, Y., Kyser, T.K., Dix, G.R., & Collins, L.B. (2004). The importance of changing oceanography in controlling late Quaternary carbonate sedimentation on a high-energy, tropical, oceanic ramp: North-western Australia. *Sedimentology, 51*, 1179-1205.

Jenkins, D.G., & Srinivasan, M.S. (1986). Cenozoic planktonic foraminifers from the equator to the sub-Antarctic of the southwest Pacific. In: Kennett, J.P., & von der Borch, C.C. (eds). *Initial Reports of the Deep Sea Drilling Project,* 90. US Government Printing Office, Washington D.C. 795-834.

631 Jones, H.A. (1973). Marine geology of the northwest Australian continental shelf. Bureau of
632 Mineralogical Resources, *Geologicaly and Geophysical Bulletin, 136*, 1A-102.
633
634 Karas, C., Nurnberg, D., Gupta, A.K., Tiedemann, R., Mohan, K., & Bickert, T. (2009). Mid-Pliocene
635 climate change amplified by a switch in Indonesian subsurface throughflow. *Nature Geoscience,*
636 *2*, 434–438.
637
638 Karas, C., Nurnberg, D., Tiedemann, R., & Garbe-Schonberg, D. (2011). Pliocene Indonesian
639 Throughflow and Leeuwin Current dynamics: implications for Indian Ocean polar heat flux.
640 *Paleoceanography*, *26*. https://doi .org /10 .1029 /2010pa001949
641
642 Karatsolis, B.Th., De Vleeschouwer, D., Groeneveld, J., Christensen,B., & Henderiks, J. (2020). The
643 late Miocene – early Pliocene „Humid Interval" on the NW Australian shelf: disentangling climate
644 forcing from regional basin evolution. *Paleoceanography and Paleoclimatology,*
645 https://doi.org/10.1029/2019PA003780
646
647 Keep, M., Holbourn, A., Kunht, W. & Gallagher, S.J. (2018). Progressive Western Australian collision
648 with Asia: implications for regional orography, oceanography, climate and marine biota. *Journal*
649 *of the Royal Society of Western Australia*, *101*, 1-17.

650 Kennett, J.P. & Srinivasan, M.S. (1983). Neogene Planktonic Foraminifera: A Phylogenetic Atlas.
651 Hutchison Ross, Stroudsburg, PA, 263 pp.

652 Kotov, S., & Pälike, H. (2017). MyDTW-Dynamic Time Warping program for stratigraphical time
653 series. Paper presented at the EGU General Assembly Conference Abstracts.
654
655 Laskar, J., Robutel, P., Joutel, F., Gastineau, M., Correia, A., & Levrard, B. (2004). A long-term
656 numerical solution for the insolation quantities of the Earth. *Astronomy and Astrophysics*, *428*,
657 261–285.
658
659 Lazarus, D., Hilbrecht, H., Spencer-Cervato, C., & Thierstein, H.R. (1995). Sympatric speciation and
660 phyletic change in *Globorotalia truncatulinoides*. *Paleobiology, 21*, 28-51.
661
662 Lisiecki, L. E., & Lisiecki, P. A. (2002). Application of dynamic programming to the correlation of
663 paleoclimate records. Paleoceanography, 17(4), 1049, doi:10.1029/2001PA000733
664
665 Lisiecki, L.E., & Raymo, M.E. (2005). A Pliocene-Pleistocene stack of 57 globally distributed benthic
666 δ^{18}O records. *Paleoceanography*, *20*, PA1003. doi: 10 .1029 /2004PA001071
667
668 Lisiecki, L. E., & Herbert, T. D. (2007). Automated composite depth scale construction and estimates
669 of sediment core extension. *Paleoceanography, 22*(4). 10.1029/2006PA001401
670
671 Longley, I.M., Buessenschuett, C., Clydsdale, L., Cubitt, C.J., Davis, R.C., Johnson, M.K., Marshall,
672 N.M., Murray, A.P., Somerville, R., Spry, T.B., & Thompson, N.B. (2002). The North West Shelf
673 of Australia—a Woodside perspective. In: Keep, M., & Moss, S.J. (eds). *The Sedimentary*
674 *Basins of Western Australia 3*. Proceedings of the Petroleum Exploration Society of Australia
675 Perth 27-88.
676
677 Lourens, L.J., Hilgen, F.J., Laskar, J., Shackleton, N.J., & Wilson, D. (2004). The Neogene period. In:
678 Gradstein, F., Ogg, J., and Smith, A.G. (eds). *A Geological Time Scale 2004*. Cambridge University
679 Press, Cambridge, 409-440.
680

McCaffrey, J., Wallace, M.W., & Gallagher, S.J. (2020). A Cenozoic Great Barrier Reef on Australia's North West Shelf. *Global and Planetary Change*, *184*, 1030148. https://doi.org/10.1016/j.gloplacha.2019.103048

Mitchum, R.M., Jr., Vail, P.R., & Sangree, J.B. (1977). Seismic stratigraphy and global changes of sea level, part 6: stratigraphic interpretation of seismic reflection patterns in depositional sequences. *Seismic Stratigraphy – Application to Hydrocarbon Exploration, 165*, 117‑134. doi:10.1038/272400a0

Moss, G.D., Cathro, D.L., & Austin Jr, J.A. (2004). Sequence biostratigraphy of prograding clinoforms, northern Carnarvon Basin, Western Australia: a proxy for variations in Oligocene to Pliocene global sea level? *Palaios, 19*, 206–226

Norris, R.D. (1998). Planktonic foraminifer biostratigraphy: eastern equatorial Atlantic, Leg 159. In: Mascle, J., Lohmann, G.P., and Moullade, M. (eds). *Proceedings of the Ocean Drilling Program. Scientific Results, 159*. College Station, TX. 445-479

Petrick, B., Reuning, L., & Martínez-García, A. (2019). Distribution of glycerol dialkyl glycerol tetraethers (GDGTs) in microbial mats from Holocene and Miocene sabkha sediments. *Frontiers in Earth Science, 7*(310). doi: 10.3389/feart.2019.00310

Power, M. (2008). Miocene carbonate reef complexes in the Browse Basin and the implication for drilling operations. *Australian Petroleum Production and Exploration Association Journal, 48*, 115–132.

Rosenthal, Y., Holbourn, A.E., Kulhanek, D.K., Aiello, I.W., Babila, T.L., Bayon, G., Beaufort, L., Bova, S.C., Chun, J.-H., Dang, H., Drury, A.J., Dunkley Jones, T., Eichler, P.P.B., Fernando, A.G.S., Gibson, K., Hatfield, R.G., Johnson, D.L., Kumagai, Y., Li, T., Linsley, B.K., Meinicke, N., Mountain, G.S., Opdyke, B.N., Pearson, P.N., Poole, C.R., Ravelo, A.C., Sagawa, T., Schmitt, A., Wurtzel, J.B., Xu, J., Yamamoto, M., and Zhang, Y.G. (2018). Expedition 363. In Rosenthal, Y., Holbourn, A.E., Kulhanek, D.K., and the Expedition 363 Scientists, *Western Pacific Warm Pool*. *Proceedings of the International Ocean Discovery Program, 363*: College Station, TX (International Ocean Discovery Program). https://doi.org/10.14379/iodp.proc.363.101.2018

Rosleff-Soerensen, B., Reuning, L., Back, S., & Kukla, P. (2012). Seismic geomorphology and growth architecture of a Miocene barrier reef, Browse Basin, NW-Australia. *Marine and Petroleum Geology, 29*, 233–254.

R Core Team. (2014). R: A language and environment for statistical computing. R Foundation for Statistical Computing. In. Vienna, Austria.

Ryan, G.J., Bernardel, G., Kennard, J.M., Jones, A.T., Logan, G.A., & Rollet, N. (2009). A precursor extensive Miocene reef system to the Rowley Shoals reefs, WA: evidence for structural control of reef growth or natural hydrocarbon seepage. *Australian Petroleum Production and Exploration Association Journal, 49*, 337–363.

Saito, T. (1976). Geologic significance of coiling direction in the planktonic foraminifer *Pulleniatina*. *Geology, 4*(5),305–309.

Sakoe, H., & Chiba, S. (1978). Dynamic programming algorithm optimization for spoken word recognition. IEEE Transactions on Acoustics, Speech, and Signal Processing, 26(1), 43-49. 10.1109/TASSP.1978.1163055

724 Sanchez, C.M., Fulthorpe, C.S., & Steel, R.J. (2012). Middle Miocene–Pliocene siliciclastic influx across
725 a carbonate shelf and influence of deltaic sedimentation on shelf construction, Northern
726 Carnarvon Basin, Northwest Shelf of Australia. *Basin Research, 24*, 664-682.

727 Scarselli, N., McClay, K., & Elders, C. (2013). Submarine slide and slump complexes, Exmouth Plateau,
728 NW Shelf of Australia, in: Keep, M., Moss, S.J. (Eds.), *The Sedimentary Basins of Western*
729 *Australia 3, Proceedings of the Petroleum Exploration Society of Australia Perth*, WA, Australia,
730 1-20.

731 Schiebel, R., & Hemleben, Ch. (2017). *Planktic foraminifers in the modern ocean*. Springer-Verlag
732 Berlin – Heidelberg. 358 pp.
733
734 Shackleton, N.J., Baldauf, J.G., Flores, J.-A., Iwai, M., Moore Jr., T.C., Raffi, I., & Vincent, E. (1995).
735 Biostratigraphic summary for Leg 138. In: Pisias, N.G., Mayer, L.A., Janacek, T.R., et al.
736 (Eds.). *Proceedings of the Ocean Drilling Program. Scientific Results*, *138*, College Station, TX
737 (Ocean Drilling Program), 517–536.
738
739 Sinha, D.K., & Singh, A.K. (2008). Late Neogene planktic foraminiferal biochronology of the ODP Site
740 763A, Exmouth Plateau, southeast Indian Ocean. *Journal of Foraminiferal Research, 38*, 251-
741 270.
742
743 Smith, R.A., Castañeda, I.S., Henderiks, J., Christensen, B.A., De Vleeschouwer, D., Renema, W.,
744 Groeneveld, J., Bogus, K., Gallagher, S.J., & Fulthorpe, C.S. (subm.). Constraining Indonesian
745 Throughflow variability across the Plio-Pleistocene using organic geochemical temperature
746 proxies from NW Australian offshore sediments. *Paleoceanography and Paleoclimatology*
747
748 Speich, S., Blanke, B., de Vries, P., Drijfhout, S, Döös, K., Ganachaud, A., & Marsh, R. (2002). Tasman
749 leakage: A new route in the global ocean conveyor belt. *Geophysical Research Letters, 29*, 55-
750 51. doi:10.1029/2001GL014586
751
752 Spencer-Cervato, C., & Thierstein, H.R. (1997). First appearance of *Globorotalia truncatulinoides*:
753 cladogenesis and immigration. *Marine Micropaleontology, 30,* 267-291.
754
755 Srinivasan, M.S., & Chaturvedi, S.N. (1992). Neogene planktonic foraminiferal biochronology of the
756 DSDP sites along the Ninetyeast Ridge, northern Indian Ocean. *Centenary of Japanese*
757 *Micropaleontology* (eds K. Ishizaki, T. Saito), 175-188.

758 Srinivasan, M.S., & Sinha, D.K. (1998). Early Pliocene closing of the Indonesian Seaway: evidence from
759 north-east Indian Ocean and tropical Pacific deep sea cores. *Journal of Asian Earth Sciences,*
760 *16*, 29-44.

761 Tagliaro, G., Fulthorpe, C., Gallagher, S., McHugh, C., Kominz, M., & Lavier, L. (2018). Neogene
762 siliciclastic deposition and climate variability on a carbonate margin: Australian Northwest
763 Shelf. *Marine Geology, 403*, 285-300.

764 Thompson, P.R., Bé, A.W.H., Duplessy, J.-C., & Shackleton, N.J. (1979). Disappearance of pink-
765 pigmented *Globigerinoides ruber* at 120,000 yr BP in the Indian and Pacific oceans. *Nature, 280*,
766 554–558.

767 Van Sebille, E., England, M.H., Zika, J.D., & Sloyan, B.M. (2012). Tasman Leakage in a fine-

768 resolution ocean model. Geophysical Research Letters, 39. doi:10.1029/2012gl051004

769 Wade, B.S., Pearson, P.N., Berggren, W.A., & Pälike, H. (2011). Review and revision of Cenozoic
770 tropical planktonic foraminiferal biostratigraphy and calibration to the geomagnetic polarity
771 and astronomical time scale. Earth-Science Reviews, 104, 111–142.

772 Wallace, M.W., Condilis, E., Powell, A., Redfearn, J., Auld, K., Wiltshire, M., Holdgate, G.R., &
773 Gallagher, S.J. (2003). Geological controls on sonic velocity in the Cenozoic carbonates of the
774 Northern Carnarvon Basin, North West Shelf, Western Australia. *Australian Petroleum*
775 *Production and Exploration Association Journal, 43*, 385-399.

776 Zachiariasse, W.J. (1992). Neogene planktonic foraminifers from Sites 761 and 762 off northwest
777 Australia. *Proceedings of the Ocean Drilling Program. Scientific Results, 122,* 665–681.

778 Zachos, J.C., Pagani, M., Sloan, L., Thomas, E., & Billups, K. (2001). Trends, rhythms, and aberrations
779 in global climate 65 Ma to present: *Science*, *292*, 686–693. doi: 10 .1126 /science
780 .1059412.
781

782 **Tables**

783 Table 1) Overview of IODP sites and industry wells used in this study.

784 Table 2) Shipboard biostratigraphic age model for IODP Site U1463 in comparison with the updated
785 biostratigraphic datums based on the new astronomically-tuned age-depth model, as well as the
786 geological timescale, ODP Site 763, and Deep Sea Drilling Program (DSDP) sites 214 and 586.

787 Table 3) Tie-points (WMSF depth scale for IODP sites; bRT depth scale for industry wells) for
788 biostratigraphic datums at IODP Site U1463 to other sites on the NWS.

789 Table 4) Tie-points of reconstructed age vs sediment depth based on benthic stable oxygen and
790 carbon isotopes of IODP Site U1463.

791

792 **Figure Captions**

793 Figure 1) Map of the northwest shelf of Australia with relevant sites, both (I)ODP and industry wells,
794 used in this study (black stars) with IODP Site U1463 as reference site (red star). Additional sites
795 discussed in the text are also indicated (black dots). Orange line indicates the seismic profile
796 connecting the different site locations; green line depicts the downslope profile including IODP Site
797 U1463. Additional main features of the NWS like basin boundaries, existing and paleo-reefs are
798 marked.

799 Figure 2) Construction of the astronomically-tuned age model for IODP Site U1463. A) Expression of
800 the 405-kyr eccentricity cycle on the $\delta^{13}C_{benthic}$ record of IODP Site U1463 in the depth domain; B)
801 Sedimentation rate resulting from the new age model; C) The $\delta^{18}O_{benthic}$ record of IODP Site U1463
802 using *Uvigerina* spp. in comparison with the global benthic LR04 $\delta^{18}O$-stack (Lisiecki and Raymo,
803 2005); D) the $\delta^{13}C_{benthic}$ record of IODP Site U1463 in comparison with ETP (eccentricity – tilt –
804 precession; Laskar et al., 2004); E) TEX86 temperatures for Site U1463 (Smith et al., subm.) in
805 comparison with the global benthic LR04 $\delta^{18}O$-stack (Lisiecki and Raymo, 2005); F) Potassium content

806 based on wireline logging NGR of IODP Site U1463 (Christensen et al., 2017) in comparison with ETP
807 (Laskar et al., 2004).

808 Figure 3) Correlation of the NGR record of IODP Site U1463 with other IODP sites and industry wells.
809 A) Sediment depth (m WMSF) vs age according to the new age model for IODP Site U1463; b) NGR
810 comparison based on the NGR record of IODP Site U1463 plotted vs sediment depth. The NGR
811 records of the other sites are plotted according to their correlation to the IODP Site U1463 NGR
812 record. Tie points in the respective records to IODP Site U1463 are given as the respective depths (in
813 meters below sea floor/rig floor) noted along the record.

814 Figure 4) Alongshore seismic profile from IODP Site U1462 to IODP Site U1464 showing the main
815 seismic reflectors during the late Neogene can be followed along the NWS. Newly calibrated
816 biostratigraphic age markers and updated ages for the main reflectors are indicated. An estimation of
817 siliciclastic deposits of the Bare Formation are marked (white) showing its non-synchronous
818 deposition on the NWS; the top of the formation follows the interpretation of Tagliaro et al. (2018).
819 Letters A-D refer to the respective depth markers as shown in Figure 3. The NGR records of the
820 respective core locations are shown for comparison with the seismics.

821

822 Figure 5) Seismic profile perpendicular to the seismic profile in Fig.4 anchored at the location of IODP
823 Site U1463 showing the continuation of the main reflectors downslope, Miocene reefal carbonates
824 previously identified by McCaffrey et al. (2020), and the newly appointed Picard slide covering the
825 underlying sediment sequence. Letters A-D refer to the respective depth markers as shown in Figure
826 3. The NGR record of IODP Site U1463 is shown for comparison with the seismics.

827

828 Supplementary Figure 1) Dynamical time warping between the NGR record of IODP Site U1463 and
829 the respective NGR records of IODP Site U1462 (a), Goodwyn-2 (b), Goodwyn-6 (c), Angel-2 (d),
830 Finucane-1 (e), and IODP Site U1464. Depthscale in WMSF of IODP Site U1463 is used as reference.
831

Figure 1)

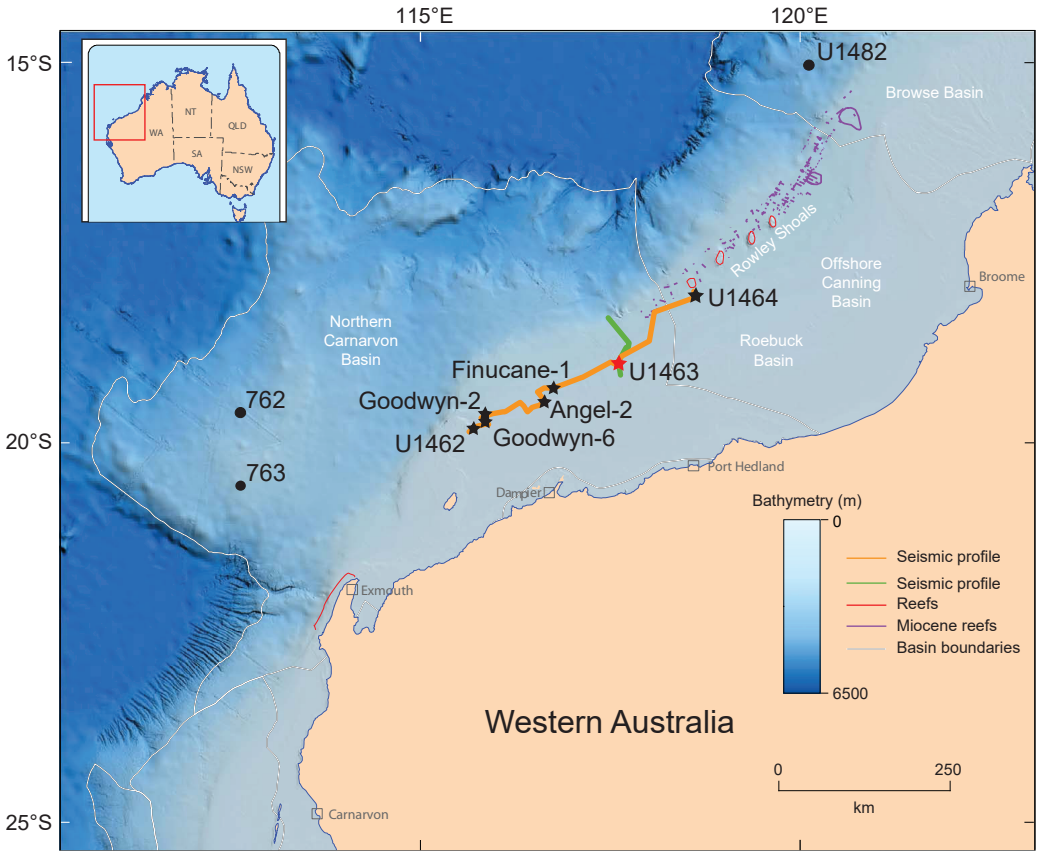
115°E
120°E
15°S
20°S
25°S
U1482
Browse Basin
Rowley Shoals
Offshore
Canning
Basin
Broome
U1464
Northern
Carnarvon
Basin
Roebuck
Basin
Finucane-1
U1463
762
Goodwyn-2
Angel-2
U1462
Goodwyn-6
763
Port Hedland
Dampier
Exmouth
Carnarvon
Bathymetry (m)
0
6500
Seismic profile
Seismic profile
Reefs
Miocene reefs
Basin boundaries
Western Australia
0
250
km
NT
QLD
WA
SA
NSW

Figure 2)

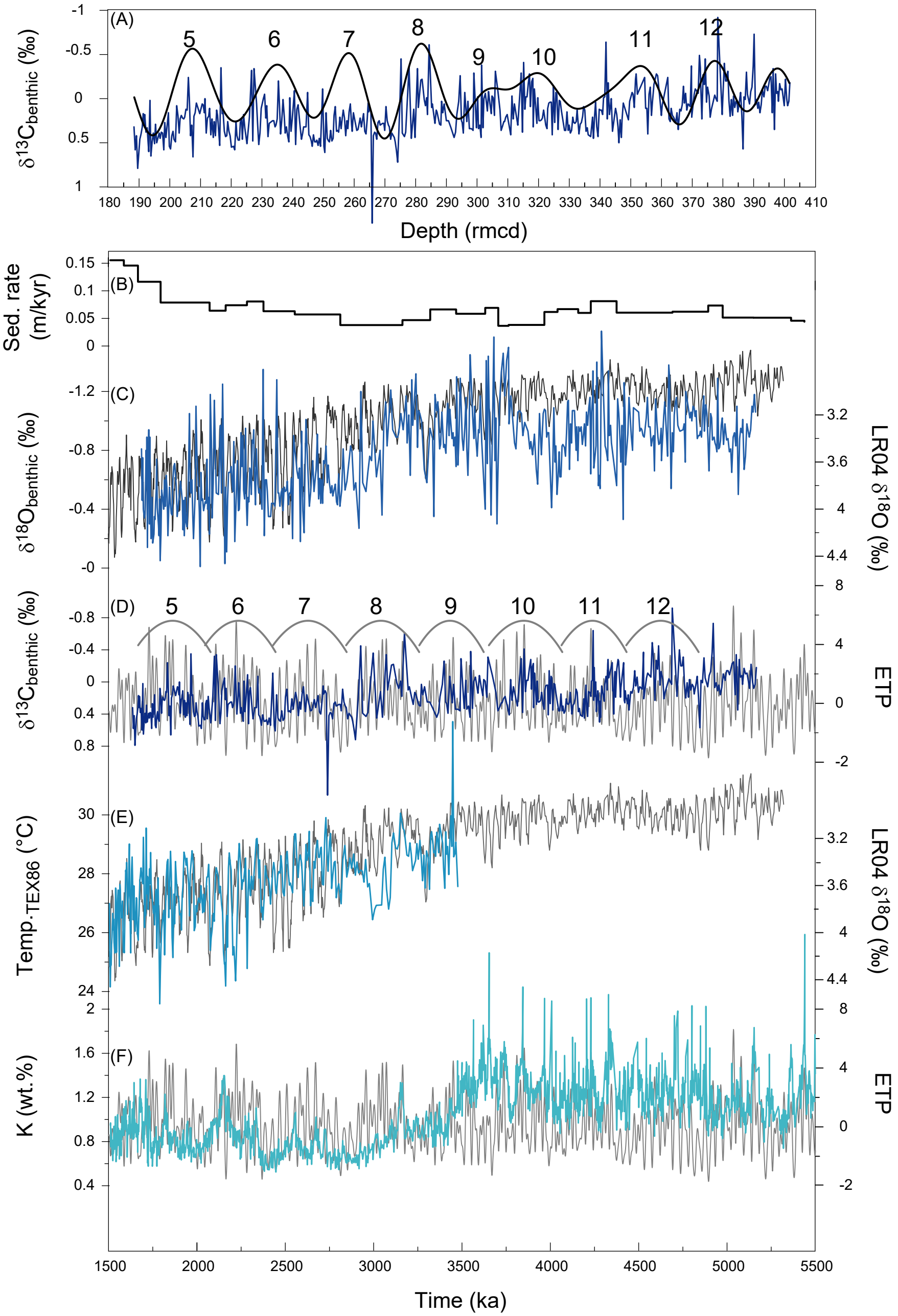
(A)
δ13Cbenthic (‰)
-1
-0.5
0
0.5
1
5
6
7
8
9
10
11
12
180 190 200 210 220 230 240 250 260 270 280 290 300 310 320 330 340 350 360 370 380 390 400 410
Depth (rmcd)
(B)
Sed. rate (m/kyr)
0.15
0.1
0.05
0
(C)
δ18Obenthic (‰)
-1.2
-0.8
-0.4
-0
(D)
δ13Cbenthic (‰)
-0.8
-0.4
0
0.4
0.8
ETP
3.2
3.6
4
4.4
LR04 δ18O (‰)
8
4
0
-2
(E)
Temp.TEX86 (°C)
30
28
26
24
2
(F)
K (wt.%)
1.6
1.2
0.8
0.4
1500 2000 2500 3000 3500 4000 4500 5000 5500
Time (ka)

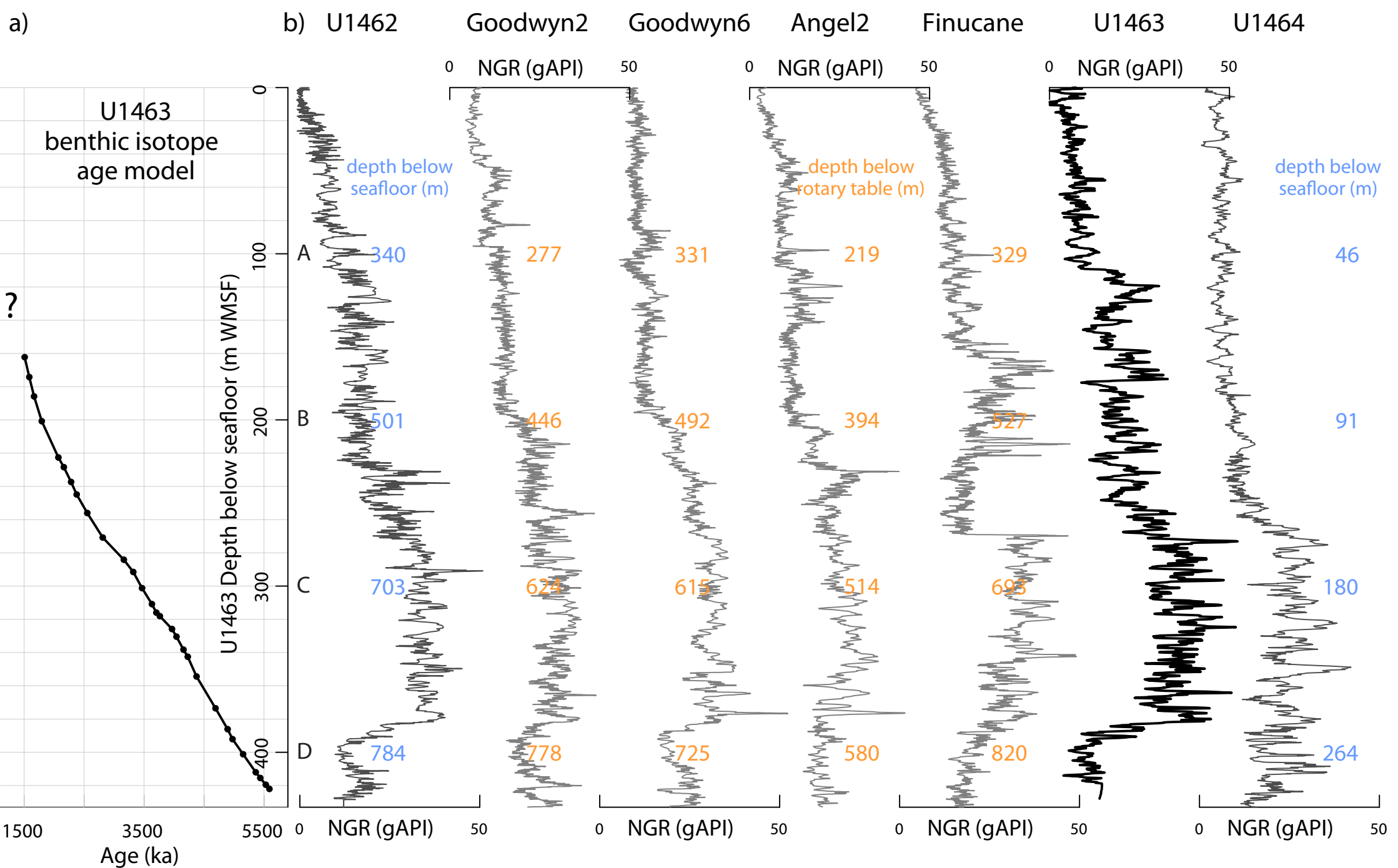
a)
b)
U1462
Goodwyn2
Goodwyn6
Angel2
Finucane
U1463
U1464
U1463
benthic isotope
age model
?
U1463 Depth below seafloor (m WMSF)
0
100
200
300
400
1500
3500
5500
Age (ka)
NGR (gAPI)
0
50
depth below
seafloor (m)
depth below
rotary table (m)
A
B
C
D
340
501
703
784
277
446
624
778
331
492
615
725
219
394
514
580
329
527
693
820
46
91
180
264

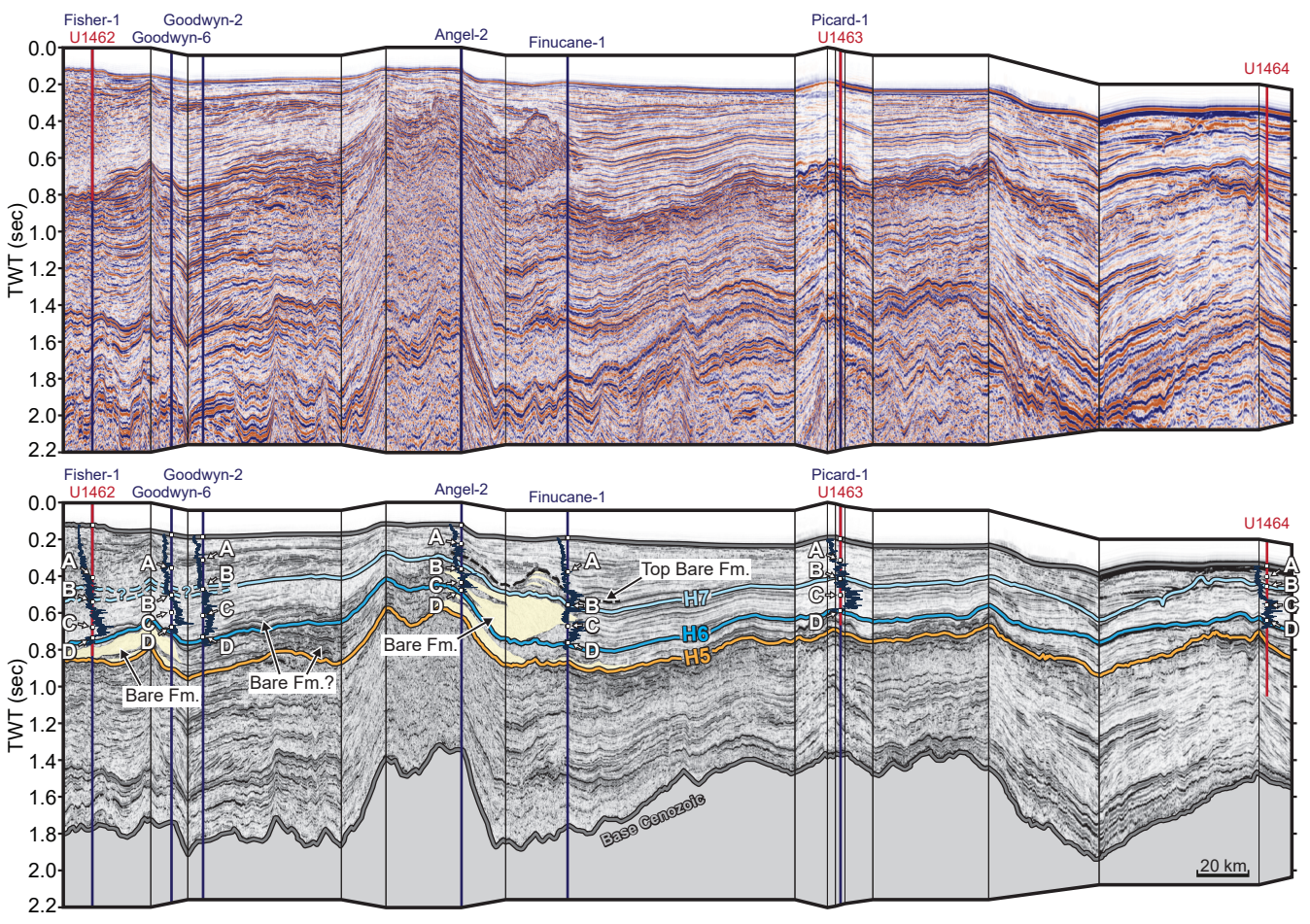
Fisher-1
U1462
Goodwyn-2
Goodwyn-6
Angel-2
Finucane-1
Picard-1
U1463
U1464
TWT (sec)
0.0
0.2
0.4
0.6
0.8
1.0
1.2
1.4
1.6
1.8
2.0
2.2
A
B
C
D
Top Bare Fm.
H7
H6
H5
Bare Fm.
Bare Fm.?
Base Cenozoic
20 km

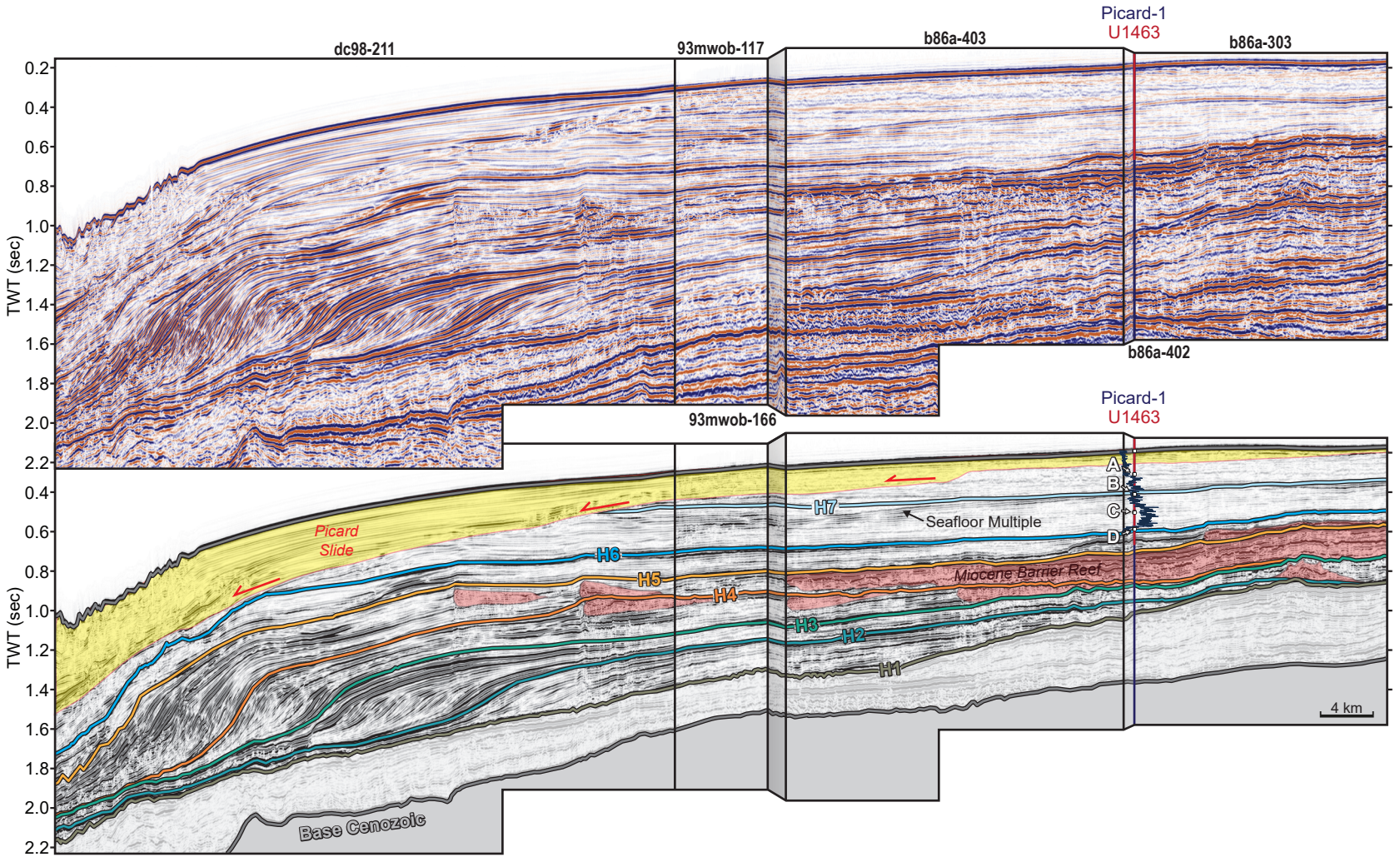
dc98-211
93mwob-117
b86a-403
Picard-1
U1463
b86a-303
b86a-402
93mwob-166
Picard-1
U1463
TWT (sec)
0.2
0.4
0.6
0.8
1.0
1.2
1.4
1.6
1.8
2.0
2.2
Picard
Slide
H7
Seafloor Multiple
H6
H5
H4
Miocene Barrier Reef
H3
H2
H1
A
B
C
D
4 km
Base Cenozoic